

In Vivo Tracking of the Degradation of Mesoporous Silica through ^{89}Zr Radio-Labeled Core–Shell Nanoparticles

Elisa Bindini, Maria de los Angeles Ramirez, Xabier Rios, Unai Cossío, Cristina Simó, Vanessa Gomez-Vallejo, Galo Soler-Illia, Jordi Llop,* and Sergio E. Moya*

While mesoporous silica nanoparticles (MSNs) are extensively studied as high-potential drug delivery platforms, the successful clinical translation of these nanocarriers strongly depends on their biodistribution, biodegradation, and elimination patterns in vivo. Here, a novel method is reported to follow the in vivo degradation of MSNs by tracking a radioactive label embedded in the silica structure. Core–shell silica nanoparticles (NPs) with a dense core and a mesoporous shell are labeled with low quantities of the positron emitter ^{89}Zr , either in the dense core or in the mesoporous shell. In vivo positron emission tomography imaging and ex vivo organ measurements reveal a remarkable difference in the ^{89}Zr biodistribution between the shell-labeled and the core-labeled NPs. Release of the radiotracer from shell-labeled NPs is used as a probe of the extent of silica dissolution, and a prompt release of the radioisotope is observed, with partial excretion already in the first 2 h post injection, and a slower accumulation in bones over time. On the other hand, when ^{89}Zr is embedded in the nanoparticle core, the biodistribution remains largely unchanged during the first 6 h. These findings indicate that MSNs have fast, hour-scale, degradation kinetics in vivo.

1. Introduction

Over the past few decades, nanomaterials have pushed forward the frontiers of diagnostics and therapy.^[1–9] Many nanoparticle platforms have been exploited as drug delivery vehicles, such as inorganic nanoparticles,^[10] liposomes,^[11,12] and polymer NPs.^[13,14] However, a major drawback for the biomedical application of nanoparticles is that often they are not biodegradable and have limited body clearance, accumulating in the body with undesired consequences.^[15]

Among inorganic nanoparticles, mesoporous silica nanoparticles (MSNs) deserve special attention thanks to their uniform and tuneable pore size, large surface area, and easy functionalization of pores and surface.^[16–20] The porous structure of MSNs can be chemically engineered by relatively simple methods and pores can be filled with several types of drugs^[21–25] or therapeutics such as RNA,^[26] DNA,^[27] or proteins^[28] for delivery. Silica is generally recognized as being safe by the U.S. Food and Drug Administration (FDA)^[29] with

silica-based nanocarriers undergoing clinical trials.^[30,31] Several reports investigate the effect of size, shape, and surface chemistry on MSNs biocompatibility and biodistribution.^[32–39] MSNs have an advantage over other porous materials, as they can degrade under physiological conditions. Moreover, degradation plays a fundamental role in the delivery of encapsulated drugs.^[40] Nevertheless, the mechanism and kinetics of degradation of MSNs in biologically relevant conditions are still controversial, as they largely depend on particle concentration, MSN size, morphology, porosity, degradation medium, and condensation degree.^[41]

Amorphous silica is unstable in aqueous environments and it hydrolyses forming soluble silicic acid and silicate oligomers. The kinetics of this reaction is limited by saturation as silica can nucleate and re-precipitate from saturated media, ceasing dissolution.^[42,43] Moreover, this dynamic equilibrium may lead to pore obstruction in the case of mesoporous silica, further impacting on its degradation behavior as the surface area will decrease.^[44,45] In fact, one of the main parameters controlling the degradation kinetics of mesoporous silica is its surface area.^[32,45,46] In addition, pH and temperature also greatly affect silica dissolution.^[47,48] The different parameters involved in silica dissolution lead to a huge variety of possible scenarios

Dr. E. Bindini, M. d. I. A. Ramirez, C. Simó, Dr. S. E. Moya

Soft Matter Nanotechnology Group

CIC biomaGUNE

Basque Research and Technology Alliance (BRTA)

Paseo Miramón 182, San Sebastián, Guipúzcoa 20014, Spain

E-mail: smoya@cicbiomagune.es

M. d. I. A. Ramirez, Prof. G. Soler-Illia

Instituto de Nanosistemas

UNSAM

CONICET

Avenida 25 de Mayo 1021, San Martín, Buenos Aires 1650, Argentina

Dr. X. Rios, Dr. U. Cossío, C. Simó, Dr. V. Gomez-Vallejo, Dr. J. Llop

Radiochemistry and Nuclear Imaging Group

CIC biomaGUNE

Basque Research and Technology Alliance (BRTA)

Paseo Miramón 182, San Sebastián, Guipúzcoa 20014, Spain


E-mail: jlllop@cicbiomagune.es

Dr. J. Llop

Centro de Investigación Biomédica en Red – Enfermedades

Respiratorias (CIBERES)

Av. Monforte de Lemos, 3–5, Madrid 28029, Spain

 The ORCID identification number(s) for the author(s) of this article can be found under <https://doi.org/10.1002/smll.202101519>.

DOI: 10.1002/smll.202101519

and to inconsistent results for the kinetics of silica degradation in physiological buffers or biological media. Silica dissolution has been indeed reported to last between a few hours and several days depending on the experimental conditions and MSN properties.

In several studies, MSN degradation was observed over 7–15 days, reaching a maximum rate in the first 2 days.^[33,37,49–51] In other cases, MSNs were claimed to be stable over 20 days in simulated body fluid (SBF).^[52] However, studies made on mesoporous thin films indicate degradation kinetics on the time scale of 2–6 h.^[42,46,53] These huge discrepancies are due to large extent to the large variability of particle concentration and medium composition in the different studies. In fact, as investigated by He et al.,^[45] MSNs display a rapid degradation phase in physiologic buffers that lasts ≈ 2 h, dissolving from 35% to 85% of the starting material, depending on the concentration. If the concentration of MSN is above the solubility limit of silica, $145 \mu\text{g mL}^{-1}$ in water at 37°C for silicic acid,^[47] free silicon species saturation is quickly reached and the silica begins to re-precipitate, apparently halting the dissolution process. If the MSN concentration is far below the solubility limit for silica, re-precipitation is avoided, and MSNs degrade in a few hours. Working at 0.1 mg mL^{-1} , 85% of the starting MSN material is dissolved in 2 h in SBF before re-precipitation occurs. However, only 35% of the material is dissolved when working at 0.5 mg mL^{-1} .^[45] In many MSN studies related to stability, the working concentration is generally above 0.1 mg mL^{-1} , often approaching 1 mg mL^{-1} , which may explain the reported stability of several days. The different degradation conditions (concentration, media) for MSNs and outcome (% of degradation and degradation time) *in vitro* described in literature have been summarized in Table S1 in the Supporting Information.

A fundamental issue when studying the degradation of drug delivery vehicles is to consider final conditions in a biological environment. If MSNs are injected to animals, the concentrations employed are always very far from saturation conditions, typically 0.02 mg mL^{-1} . Moreover, *in vivo*, nanoparticles are exposed to a flowing media, which removes products of dissolution and should reduce re-precipitation and aggregation. Therefore, we might expect *in vivo* degradation behavior on an hour-scale, probably impeded with respect to SBF by the presence of proteins and other biomolecules that adsorb onto the particle surface.^[46,49]

All studies carried out on MSN degradation up to now have been performed *in vitro*, trying to simulate *in vivo* conditions. Despite almost 20 years of MSN related studies, investigations focused on *in vivo* degradation of MSNs for drug delivery can be hardly found in the literature. The uncertainty surrounding their degradation behavior is greatly restricting MSN translation from laboratories to clinical use. There are several *in vivo* studies on biodistribution and clearance of MSNs,^[18,20,39,54–58] but to the best of our knowledge, no dedicated work addressing MSN degradability *in vivo* has been reported until now. Monitoring MSN degradation *in vivo* following systemic delivery poses several technical difficulties. The *in vivo* visualization and quantification of nanomaterials is highly nontrivial. Techniques like inductively coupled mass spectroscopy, which is frequently used for the quantification of element content in organs, require animal sacrifice and are not capable of distinguishing particulate silica from ions, providing information

only on the total silica content. Fluorescence imaging can be used for tracing fluorescently labeled NPs *in vivo*; however, it is not quantitative and is difficult to translate to large animal species or humans.

For a quantitative evaluation of the distribution of NPs in bodily organs *in vivo*, nuclear imaging techniques such as positron emission tomography (PET) or single photon emission computerized tomography (SPECT), which detect activity from radionuclides incorporated in the NPs or linked to their surface, are ideally suited. Relative activity per organ can be related to the amount of nanomaterials in the organs from an initial dose/activity supplied. However, nanomaterial imaging/quantification in PET/SPECT relies on the fact that the tracer is always associated with the NPs. *A priori*, PET/SPECT techniques cannot distinguish between free radionuclide and the radionuclide associated with the NPs. However, one can expect that the biodistribution of detached radionuclides in the form of ions or organic molecules may significantly differ from that of the labeled NPs. Hence, a means to distinguish between free radionuclide coming from dissolution of the mesoporous NPs and radionuclide bound to the mesoporous nanoparticles (not dissolved MSNs) would be to ensure that in one case the nanoparticle does not dissolve, thereby providing information on nanoparticle biodistribution, while in the other it does dissolve. As the silica dissolution rate depends on surface area, mesoporous silica degrades much faster than dense silica. A core–shell nanoparticle with a core of dense silica and a shell of mesoporous silica, which could be either labeled in the core or in the shell, could provide a means to distinguish between free and nanoparticle bound radionuclide. Radiolabeling at the core would provide information about the biodistribution of the nanoparticles, and if the radionuclide is located in the mesoporous shell, a different pattern of biodistribution from the core would mean that the mesoporous structure has degraded. Based on this idea, we prepared core–shell nanoparticles with a dense silica core and a mesoporous shell, and we labeled either the core or the shell with Zirconium-89 (^{89}Zr) as sketched in **Figure 1a**. This positron emitter ($t_{1/2} = 78.4$ h, positron energy $\beta^+_{\text{avg}} = 396$ keV) is particularly suitable for chelator-free labeling of silica. This is because Zr can integrate with the network of silica^[59,60] and it bonds easily to the surface silanols following chelator-free labeling procedures.^[57,58,61] Core–shell MSNs with ^{89}Zr on the core, and core–shell MSNs with the label in the shell are identical, differing only in the location of the label and can be expected to have the same fate. By designing this core–shell labeling strategy, we show that we are able to discriminate the fate of the nanoparticle from that of the degradation products. Our results provide a first *in vivo* evaluation of the degradation of mesoporous silica and introduce fundamental knowledge for the design and evaluation of the drug delivery potential of mesoporous materials.

2. Results and Discussion

2.1. Morphology and Mesostructure of Core and Core–Shell Silica Particles

Transmission electron microscopy (TEM) images of dense core silica nanoparticles clearly indicate that they have uniform

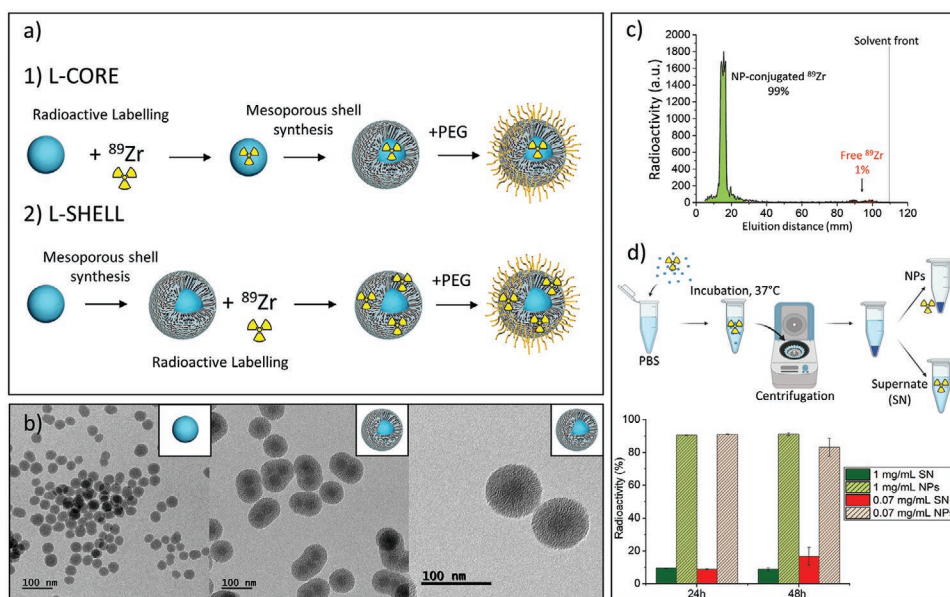


Figure 1. Synthesis and characterization of ^{89}Zr -labeled core-shell SiO_2 nanoparticles: a) Scheme of the multi-step synthesis of L-CORE and L-SHELL NPs; b) TEM images of the dense silica core and the core-shell NPs; c) iTLC chromatogram of ^{89}Zr -labeling reaction, using EDTA $50 \times 10^{-3} \text{ M}$ (pH = 5) as eluent. Nonbound ^{89}Zr is eluted with the solvent while ^{89}Zr bound to nanoparticles is retained with NPs on the silica thin layer; d) radiochemical stability test in PBS, 37 °C. Green colors represent 1 mg mL $^{-1}$ concentration of NPs, red colors represent 0.07 mg mL $^{-1}$. Patterned bars represent radioactivity values of nanoparticles, while nonpatterned bars are chosen for supernatant.

nanoparticle sizes with a diameter of about 40 nm and a regular spherical morphology (Figure 1b, left and Figure S1, Supporting Information). Following the synthesis of the dense core, a mesoporous shell was fabricated via a standard templated sol-gel approach, resulting in a clear core-shell structure (Figure 1b, middle and right and Figure S2, Supporting Information), where the 40 nm silica core is coated with a 20 nm shell of mesoporous silica. The size of core-shell nanoparticles is 80 nm in diameter, with a small percentage of the multicore nanoparticles approaching 120 nm. Still, these nanoparticles remain in the size-range in which rapid lung and spleen accumulation in vivo is limited.^[62] The mesoporous structure, visible by TEM, was confirmed by nitrogen adsorption-desorption isotherms, which showed an average pore diameter of 2.5 nm (Figure S4, Supporting Information), typical of cetyltrimonium bromide (CTAB)-templated materials. The calculated Brunauer-Emmett-Teller surface area was 188 m 2 g $^{-1}$.

The synthesized core-shell NPs were coated with a polyethylene glycol (PEG) layer, using (3-aminopropyl)triethoxysilane (APTES) as the silane coupling agent to incorporate active amine groups on the silica surface. These APTES-coated nanoparticles were then reacted with *N*-succinimidyl ester of hydroxyl PEG (HO-PEG5K-NHS).

2.2. Chelator-Free ^{89}Zr Labeling and In Vitro Stability Tests

The chelator-free labeling procedure relies on the strong interaction between deprotonated silanol groups present on the silica surface (hard Lewis base) and the Zr^{4+} ions (hard Lewis acid) to ensure stable labeling of silica without the use of organic linkers, which may be cleaved in vivo. Labeling conditions

were chosen according to reported studies of ^{89}Zr labeling on silica MSNs, which evidenced a dependence on time and temperature of the labeling yield.^[57] Our results show that about 99% ^{89}Zr labeling yield was achieved after 1 h of incubation in HEPES (4-(2-hydroxyethyl)-1-piperazineethanesulfonic acid) at 70 °C (Figure 1c).

In order to perform the in vivo investigation of the degradation process, we prepared two different batches of nanoparticles. The first batch (core-labeled; from now on, L-CORE) incorporated the radionuclide ^{89}Zr on the dense core, i.e., dense silica NPs were exposed to ^{89}Zr before the shell synthesis; while the second batch of particles (shell-labeled; from now on, L-SHELL) was labeled via incorporation of the radionuclide in the mesoporous shell, i.e., after the synthesis of core-shell NPs. To verify the radiochemical stability of the radio-labeled nanoparticles, L-SHELL NPs were suspended in phosphate-buffered saline (PBS) at 37 °C for 24 and 48 h, under shaking. After this treatment, > 90% of the starting radioactivity (decay-corrected) was found on the nanoparticles and only 10% was found in the supernatant after 24 h, even at an NP concentration of 0.07 mg mL $^{-1}$ (i.e., slightly below saturation), as shown in Figure 1d. After 48 h, the percentage of radionuclide attached to the NPs remains unaltered at 1 mg mL $^{-1}$ (above saturation limit), while a slight release is observed at 0.07 mg mL $^{-1}$ (below saturation limit), probably due to partial silica dissolution. These results suggest that the radio-labeling strategy is robust and the radionuclide does not easily leach away unless the nanoparticle degrades. Following these results, the presence of free Zr in vivo can be directly correlated with silica dissolution, as the radionuclide is not released from intact nanoparticles but can be detected in the supernatant when degradation of mesoporous silica occurs.

2.3. In Vivo Degradation and Biodistribution Study

Next, we tackled the investigation of the degradation of the NPs in vivo, using L-SHELL and L-CORE NPs. Based on the extensive literature on mesoporous silica degradation, a fast silica hydrolysis in vivo during the first 24 h post-injection could be expected.

The labeled NPs were injected intravenously and PET imaging sessions were carried out at different times after administration. Visual inspection of PET images showed a different distribution profile for L-CORE and L-SHELL nanoparticles (**Figure 2**). Coronal maximum intensity projections PET images obtained at $t = 10$ min and 2 h periods clearly show that irrespectively of the position of the radiolabel and the time point, major uptake occurs in the liver and the spleen, as expected for NPs in this size range, due to sequestration and retention by the mononuclear phagocytic system. However, at longer times (24 and 48 h after administration) mice injected with L-SHELL particles clearly show accumulation of radioactivity in the bones, as observed in axial slices. Additionally, accumulation of radioactivity in the lungs was also observed at $t = 10$ min and 2 h. Instead, mice injected with L-CORE nanoparticles do not show any visible accumulation of radioactivity in the bones or any organs other than the spleen and liver over the whole duration of the study. The presence of ^{89}Zr in bones after administration of L-SHELL nanoparticles is indicative of the shell degradation and consequent release of the radionuclide, as: i) previous works have demonstrated that the free ^{89}Zr is preferentially uptaken in bones, where it binds to phosphates,^[63] while NPs do not accumulate in bones^[56] and ii) ^{89}Zr -labeled nanoparticles showed excellent stability in vitro (see above), thus confirming that the release of ^{89}Zr without degradation of the shell, by diffusion, is minimal. Our results clearly point out that ^{89}Zr release and accumulation in bones can be employed as an indicator of silica dissolution kinetics.

In order to acquire accurate quantitative data on MSN degradation, we combined in vivo imaging with ex vivo studies. With that aim, animals were injected intravenously with either L-CORE or L-SHELL NPs and sacrificed at different time points: 10 min, 2, 6, 24, and 48 h, post-injection. Organs were harvested and the concentration of radioactivity in each organ was determined by gamma counting (**Figure 3**). As expected, and correlating with PET results, the highest amount of radioactivity was found in the liver and the spleen, irrespectively of the position of the label, due to sequestration by the mononuclear phagocytic system; minor accumulation was observed in the heart and kidneys.^[62,64–67] Significant differences between L-CORE and L-SHELL nanoparticles were observed for the heart, the intestine, the kidneys, and the lungs. While low uptake values in these organs were observed for L-CORE NPs, significantly higher values were observed for L-SHELL, peaking at 10 min (heart, intestine, and kidneys) and 2 h (lungs) after administration and progressively decreasing afterward. These results suggest that, in the case of L-SHELL nanoparticles, ^{89}Zr is rapidly distributed in the blood and accumulated at short times mainly in the intestine and kidneys, and to lesser extent in the lungs. After 2 h, activity decreases in the intestine and kidneys while it increases in the lungs. At longer times, activity significantly decreases, remaining practically constant for

L-SHELL NPs, prior to elimination and/or ^{89}Zr activity accumulation in the bones. As the degradation of the mesoporous silica shell does not affect ^{89}Zr stability for L-CORE nanoparticles, we observe very stable values in all organs in the case of core-labeled nanoparticles.

A closer look at the values found in urine and bones (**Figure 3**) reveals some interesting trends. The presence of radioactivity in both urine and bones is a consequence of nanoparticle degradation, as intact nanoparticles do not accumulate in the bones and they are above the glomerular filtration limit of the kidneys. In urine, the concentration of radioactivity is very low over 48 h when L-CORE nanoparticles are administered, due to the slow degradation and release kinetics of the core to which ^{89}Zr is anchored. On the contrary, after intravenous injection of L-SHELL nanoparticles, a peak of radioactivity in urine is observed at 2 h after administration, confirming that a large amount of ^{89}Zr is released and excreted by the urinary system. A similar trend is observed in blood. Nanoparticle circulation in the blood stream is equivalent for both L-CORE and L-SHELL nanoparticles, since both L-CORE and L-SHELL are identical apart from the position of the label and both were administered in equal activity doses and by the same administration route. Therefore, the higher presence of radioactivity in the blood for L-SHELL nanoparticles can only be explained as a consequence of the release of ^{89}Zr associated with mesoporous silica degradation from nanoparticles accumulated in other organs.

It is interesting to note that radioactivity in the femur follows an inverse trend when compared to urine and blood. While radioactivity in blood peaks at $t = 2$ h after administration, activity in bones progressively increases over time. Our results support that in vivo, mesoporous silica degradation is fast. During the first 2 h post-injection, a consistent amount of ^{89}Zr is released and enters the blood stream. The radionuclide translocates to different organs such as the heart, lungs, and kidneys at short times after administration, and progressively accumulates in the bones over time, as previously reported.^[63] A large amount of the radionuclide is also quickly excreted through the urinary system. Our data are consistent with literature reports on MSNs excretion by renal clearance. This clearance pathway is rapid with high percentages of silica degradation products found in the urine of injected mice after 30 min,^[62] demonstrating that MSNs are indeed biodegradable in vivo with a fast hour-scale kinetics, as expected from in vitro data for low concentrations. The good correlation between the degradation times in vitro (from literature) and in vivo from our work in the same range of MSNs concentrations can be well appreciated in Table S1 in the Supporting Information. Lu and co-workers found that Si content in urine decreases with time, confirming fast renal clearance in the first 24 h. They also found that 94.4% of injected Si was excreted within 4 days through urine and feces.^[64] Moghaddam and co-workers found that around 20% of injected MSNs were excreted by urine in the first 24 h.^[39]

Analyzing the percentage of injected dose (ID) for every organ (without normalizing for the organ weight), global trends of biodistribution became evident (**Figure 4**). When ^{89}Zr is embedded in the mesoporous shell, after 10 min we observe 23% of the ID in the liver, 9% in the spleen, and 4% in the lungs. After 2 h, the radioactivity decreases to 17.5% of the ID

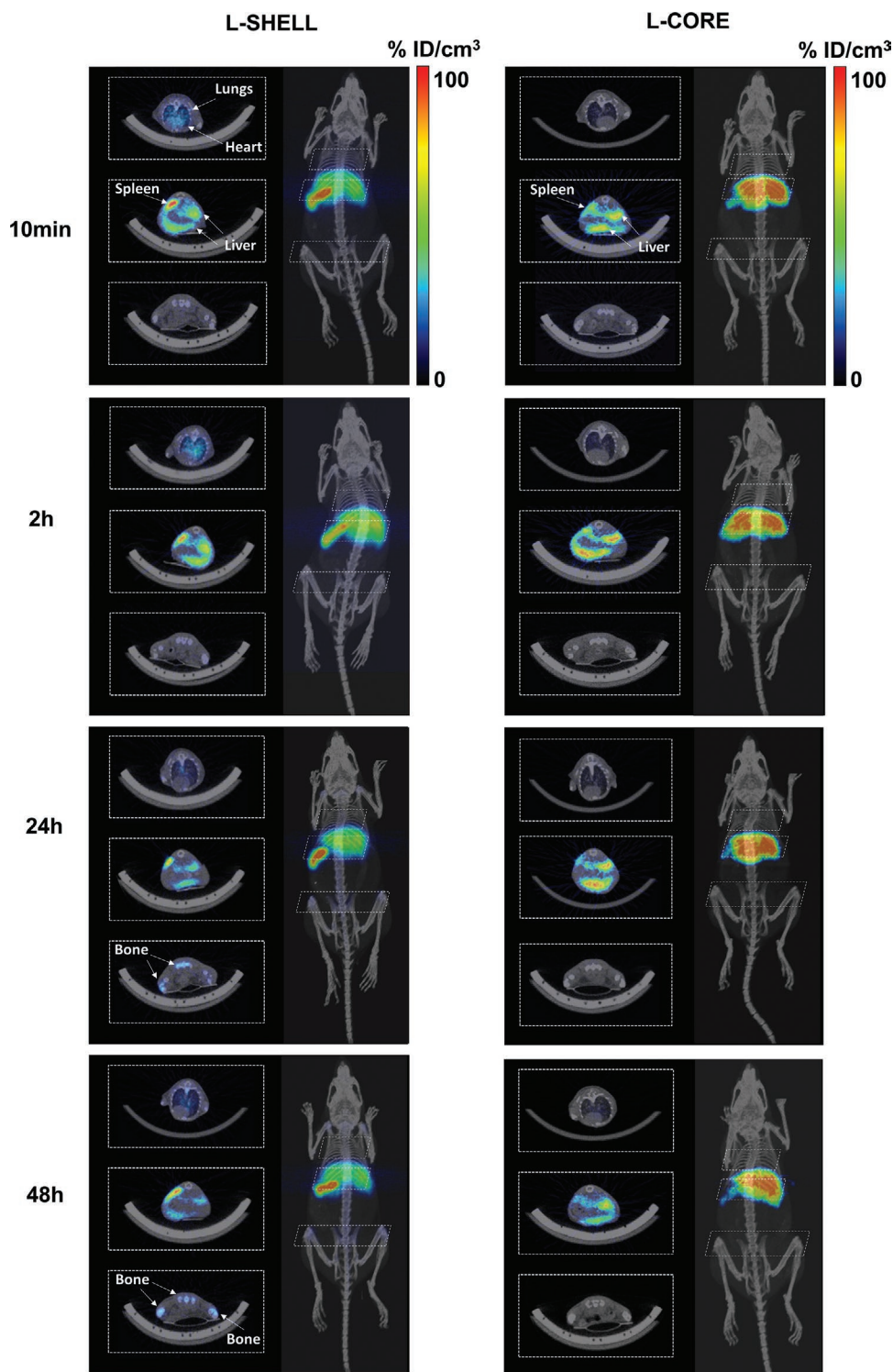


Figure 2. PET/CT images of mice injected with L-SHELL particles (left) and L-CORE particles (right) after 10 min, 2, 24, and 48 h from injection. For each time point and type of NP, whole body coronal PET maximum intensity projections have been co-registered with 3D rendered CT images. Representative axial slices, co-registered with the corresponding CT slices, are also shown. Color scale bars refer to coronal images.

and to 7% of the ID, respectively, in the liver and spleen, and increases to 8.5% of the ID in the lungs. An increase is also seen in the blood and in the femur. From these data, we can infer that MSNs become trapped in the liver and spleen in

the very first minutes and start to degrade there. The degradation products are then released and transferred to the blood, to be subsequently excreted by urine. The radionuclide ^{89}Zr is released along with silicate species and we can follow its

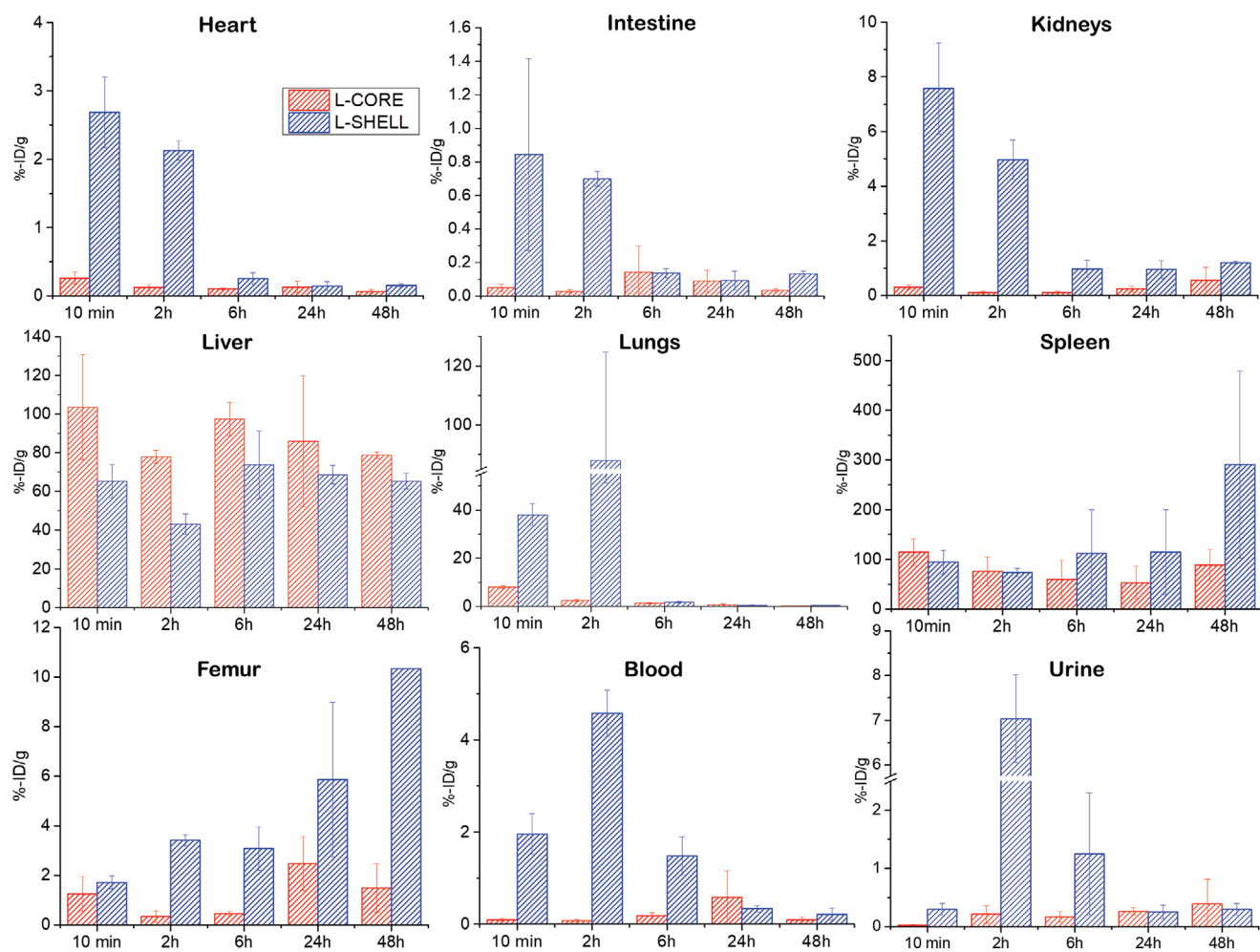


Figure 3. Percentage of injected dose per gram of organ. Results from ex vivo measurements by γ -counter. Values are represented in red for L-CORE nanoparticles and in blue for L-SHELL nanoparticles.

increase in the blood after 2 h and its diminished presence in the liver and spleen. Well-perfused blood-filled organs, such as the lungs, show enhanced accumulation of the radionuclide, which likely remains anchored to nanoparticle fragments or silicate oligomers derived from NP degradation. As already observed by He et al.,^[62] silica has a remarkable uptake in lung tissue at short times. When MSN fragments circulate for some hours, they are sent back to the liver and spleen to be excreted and we can observe an increase to 26.5% of the ID in the liver and to 9% in the spleen 6 h post-injection. After this long circulation time, the lungs are found to be almost completely clear of ^{89}Zr , which begins to accumulate in the bones. This behavior may be attributed to the fast transfer of nanoparticle fragments from the lungs to other tissues under the high local hemoperfusion rate. After 24 and 48 h, we observe a progressive decrease in activity in the liver due to MSN degradation and clearance, along with progressive accumulation of free ^{89}Zr in bones.

On the other hand, when ^{89}Zr is embedded in the core of the nanoparticles, the biodistribution remains largely unchanged in the first 6 h. Following an initially rapid uptake in the liver and spleen, mesoporous silica must degrade, and follow the

excretion path from the liver to blood and urine and from circulating blood back to the liver. However, as ^{89}Zr is unaffected by mesoporous silica degradation we do not observe any change in the radioactivity biodistribution. After 24 and 48 h, a global decrease in % ID indicates that the core begins to degrade and the majority of ^{89}Zr is likely excreted through urine and recirculates from the blood to the spleen and liver. This can be seen as only a slight increase is found in the bones, while the % ID rises in the liver and spleen. In fact, the accumulation of the radionuclide in the bones seems to take more time, as evidenced by the L-SHELL data. Nevertheless, Chen et al.^[57] found that the localization of ^{89}Zr on the surface of dense particles results in a faster release of the ^{89}Zr in vivo than for the mesoporous particles labeled with the same radioisotope. In our case, after labeling the dense silica, we assemble a mesoporous shell on top, which gives additional stability to ^{89}Zr , which is trapped between the shell and the core. We expect that the release of ^{89}Zr will only take place when the mesoporous shell is degraded and that the slow release observed for L-CORE is due mainly to the ^{89}Zr position trapped between core and shell. In the study cited in ref. [57], the mesoporous nanoparticles show a very stable

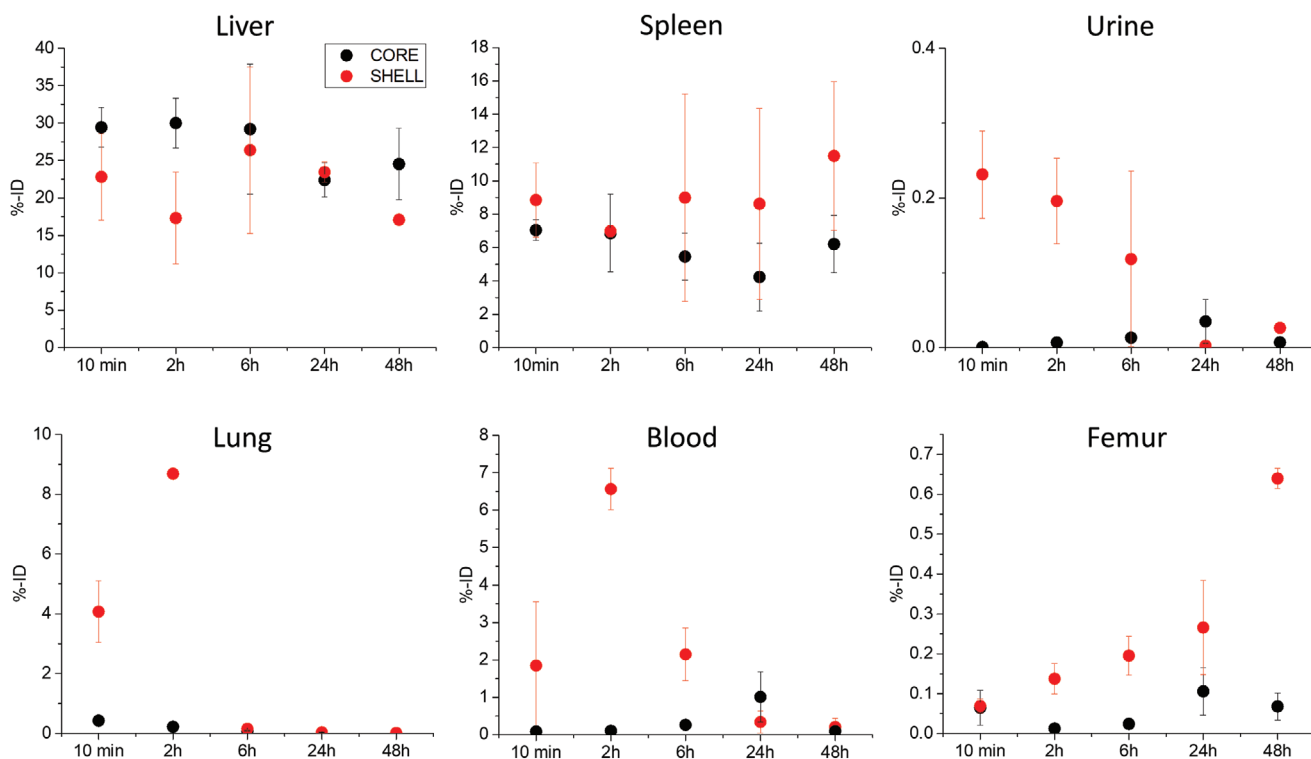


Figure 4. Percentage of injected dose (ID) for different organs: for L-SHELL nanoparticles (red dots) and for L-CORE nanoparticles (black dots). The values for blood have been calculated from the measured %ID g⁻¹, considering an average blood volume of 70 mL kg⁻¹ and a blood density of 1.057 g mL⁻¹. The values measured in urine have to be considered qualitatively, as they can greatly vary depending from the sampling (before or after mouse urination).

radio-labeling, retaining the activity in the liver for several days. Authors used MSNs of 150 nm, with long radial pores, in which ⁸⁹Zr can penetrate in depth during the labeling procedure. In these conditions, ⁸⁹Zr is confined in the mesopores, resulting in a more stable labeling. We also observe a high stability for the ⁸⁹Zr labeling in vitro, with the isotope being released only in conditions allowing the degradation of the mesoporous shell. The differences in the ⁸⁹Zr release kinetics in vivo between our NPs and the ones employed in ref. [57] can be ascribed to the different size of the NPs (larger NPs are more easily retained in the liver) and also to the depth of the mesopore structure. In fact, the mesoporous layer thickness is important because during the labeling procedure ⁸⁹Zr diffuses and binds to the surface inside the mesopores. Our nanoparticles present a very thin mesoporous shell of 20 nm that degrades much faster than a 150 nm particle, releasing ⁸⁹Zr in shorter times. Moreover, differently from our nanoparticles, mesoporous NPs were not PEGylated in Chen's work. The absence of PEG on the NPs probably results in the accumulation of proteins around the NPs, with consequent capping of the pores, both in vitro, in plasma, and the in vivo experiments. This phenomenon could greatly affect the silica degradation kinetics^[45,48] and the consequent ⁸⁹Zr release, hindering both processes. We assume that this is the main reason for the high stability and apparent absence of degradation of the mesoporous NPs reported in ref. [57]. In our work, PEGylation prevents the uptake of proteins but clearly allows for the diffusion of smaller molecules from the culture medium and degradation products.

3. Conclusion

The in vivo degradation of MSNs has been investigated through radioactive labeling with ⁸⁹Zr in two groups of identical core-shell nanoparticles, composed of a dense silica core and a mesoporous silica shell, with the radiolabel localized either in the core or in the shell. When the label is located in the mesoporous shell, the radioisotope is released promptly, following the silica degradation kinetics. When the core is labeled, the location of the radionuclide is unaffected by shell degradation and it co-localizes with the nanoparticle core. Nanoparticles are rapidly uptaken in the liver and spleen, and readily begin to degrade into silica fragments and silicate oligomers. These degradation products are transferred to the blood and are partially excreted through urine and partially re-circulated in the blood stream to the lungs before finally translocating back to the spleen and liver. This behavior is evidenced in the first 6 h after the injection of L-SHELL nanoparticles, following the pathway of ⁸⁹Zr that is released along with the nanoparticle fragments. We can state that the radioactive label is signaling the position of the degradation products and not the nanoparticles because L-CORE nanoparticles follow a different clearance pathway, as evidenced by the stable % ID in the liver and spleen over 6 h. After 24 h from the administration of L-SHELL NPs, we could detect radioactivity in the bones, which further increased at 48 h post-injection, resulting from ⁸⁹Zr accumulation. Following administration of L-CORE, only a slight increase in radioactivity is observed in the femur after

24 and 48 h by ex vivo measurements. These results point to a rapid in vivo MSN degradation that can already be seen at 2 h post-injection. We tackle here a fundamental aspect for the use of mesoporous silica NPs for biomedical application, such as their in vivo degradation kinetics; these results are of paramount importance to design efficient MSNs platforms for drug delivering and for targeting specific tissues, allowing to better control the drug release kinetics.

4. Experimental Section

Synthesis of Dense SiO₂ Cores (dSiO₂): Uniform ≈40 nm sized dense silica NPs were prepared using a Stöber method. Briefly, water (5 mL) was mixed with absolute ethanol (35 mL) and NH₃ solution (25%) (0.8 mL) and the mixture was stirred 20 min at 50 °C. Then, tetraethyl orthosilicate (TEOS, 1 mL) was added dropwise during 1 min and the reaction was kept under stirring at 50 °C for 1 h. Nanoparticles were collected by centrifugation (13 400 rpm, 15 min), washed with ethanol (x3), and dried 72 h at 60 °C.

Synthesis of Mesoporous Silica Shell dSiO₂@mSiO₂: 2 mg of dSiO₂ was suspended in a solution of ethanol (300 μL) and water (600 μL). CTAB was added (4.5 mg) and the mixture was left under stirring at r.t. for 20 min. Afterward, ammonia (10 μL) and TEOS (8 μL) were added sequentially, under stirring. After 45 min, nanoparticles were collected by centrifugation (10 000 rpm, 10 min) and washed with ethanol (x2). To remove CTAB, nanoparticles were sonicated in a NH₄NO₃ solution in ethanol (6 g L⁻¹) for 5 min (x3) and washed with ethanol (x2). To remove aggregates that may form during the reaction, a fast spin (3000 rpm, 2 min) was performed, collecting the supernatant only. An aliquot of the colloid was dried (overnight at 60 °C) and weight to calculate the concentration and nanoparticles were kept in absolute ethanol until use.

Synthesis of dSiO₂@mSiO₂-APTES: A solution of APTES in dry ethanol 0.1% v/v was prepared and kept under inert atmosphere. The dSiO₂@mSiO₂ were suspended in dry ethanol at a concentration of 1 mg mL⁻¹ and 10 μL of APTES solution 0.1% was added for each mg of NPs. Reaction was left stirring 4 h at r.t. under inert atmosphere. Nanoparticles were collected by centrifugation and washed with ethanol (x3). Successful grafting of APTES was checked by Z-potential measurements (Supporting Information).

⁸⁹Zr Labeling: [⁸⁹Zr]ZrC₂O₄ was produced in house following a standard protocol. The as-obtained 500 μL of 1 M oxalic acid containing ⁸⁹Zr (10.85 mCi, 401.5 MBq) were neutralized with 2 M sodium carbonate until pH 7–8 and the volume was adjusted to 1 mL with 0.5 M HEPES buffer (pH 7.4). 2 mg of the silica NPs (dSiO₂ or dSiO₂@mSiO₂-APTES) were dispersed in 700 μL of 0.5 M HEPES buffer and 500 μL of the freshly prepared ⁸⁹Zr solution was added and well mixed. The mixture was left to react 1 h at 70 °C. A drop of the reaction mixture was used to perform instant thin layer chromatography (iTLC), to verify the labeling yield. Stripes from commercially available instant thin layer chromatography paper impregnated with silica gel (iTLC-SG: Agilent) were used as a stationary phase and ethylenediaminetetraacetic acid (EDTA) 50 × 10⁻³ M (pH = 5) was used as mobile phase, measurements were made with a MiniGITA* TLC instrument. Afterward, nanoparticles were collected by centrifugation (13 400 rpm, 10 min) and washed with water (x3) to remove nonbound ⁸⁹Zr. Shell-labeled (L-SHELL) NPs were synthesized “in cold” conditions (without the addition of radionuclide) until the APTES grafting stage, then the label (⁸⁹Zr) was incorporated in the mesoporous shell, followed by PEG grafting. For core-labeled (L-CORE) NPs, the dense silica core was labeled with ⁸⁹Zr before the mesoporous shell synthesis and subsequent APTES and PEG grafting.

Synthesis of dSiO₂@mSiO₂-PEG: 2 mg dSiO₂@mSiO₂-APTES was suspended in PBS 10 × 10⁻³ M pH 7.4 (2 mL). NHS-PEG5K-OH (500 μg) was added and the reaction was left shaking (600 rpm) at r.t. for 45–60 min. Nanoparticles were then collected by centrifugation and washed with PBS (x3).

Nanoparticles were kept in ethanol until use. They were centrifuged and re-dispersed in PBS before injection.

NPs were imaged by transmission electron microscopy (TEM) operated on a LaB6-TEM of type JEOL JEM-1400PLUS (40–120 kV, HC pole piece) equipped with a GATAN US1000 CCD camera (2k × 2k).

Radio-Labeling Stability Test: dSiO₂@mSiO₂-PEG labeled with ⁸⁹Zr was suspended in 500 μL of PBS at 1 and 0.07 mg mL⁻¹ concentration. Samples triplicates were made and the radioactivity of each sample was measured. Nanoparticles were left shaking (630 rpm) at 37 °C for 24 and 48 h. Nanoparticles and supernatant were separated by centrifugation, collected and measured by an automatic γ-counter (2470 Wizard, Perkin Elmer) for radioactivity.

In Vivo PET Imaging of ⁸⁹Zr-Labeled dSiO₂@mSiO₂-PEG: Animals were maintained and handled in accordance with the Guidelines for Accommodation and Care of Animals (European Convention for the Protection of Vertebrate Animals Used for Experimental and Other Scientific Purposes). All animal procedures were performed in accordance with the Spanish policy for animal protection (RD53/2013), which meets the requirements of the European Union Animal Directive (2010/63/EU). Studies involving experimental animals were carried out in authorized (ES200690050402), AAALAC-accredited (Unit # 1612) animal facility, and approved by the Ethical Committee of CIC biomaGUNE (code: AE-biomaGUNE-0216), an external Ethical Committee (so-called Órgano habilitado, code: OH-16-01) and by local authorities (Diputación Foral de Guipuzkoa; code: PRO-AE-SS-059).

The final injections (100 μL, 1 mg mL⁻¹) were performed intravenously via the tail vein of healthy female mice (C57BL/6) which were anesthetized with 3–5% isoflurane (IsoFlo, Abbot Laboratories, Lake Bluff, IL, USA) in pure O₂. The average injected activity was 120 μCi (4.4 MBq). After administration, mice were placed on the eXplore Vista-CT scanner (GE Healthcare, Chicago, IL, USA) and static PET images were acquired at *t* = 10 min, 2, 6, 24, and 48 h time points. Two bed positions were defined in all cases to acquire whole body images. After each PET acquisition, a CT scan (X-ray energy: 40 kV, intensity: 140 μA) was performed for a later attenuation correction application in the image reconstruction, as well as for unambiguous localization of the radioactive signal. Random and scatter corrections were also applied to the reconstructed image (filtered back projection reconstruction algorithm was used to reconstruct all datasets). After reconstruction, PET images were analyzed using PMOD image analysis software (PMOD Technologies Ltd., Zurich, Switzerland).

In Vivo Biodistribution Study of ⁸⁹Zr-Labeled dSiO₂@mSiO₂-PEG: The average injected activity was 65 μCi (24.1 MBq) for shell-labeled NPs and 41 μCi (15.2 MBq) for core-labeled NPs. The average injected quantity was around 85 μg of NPs for each animal. Animals were anesthetized by isoflurane gas and sacrificed at 10 min, 2, 6, 24, and 48 h post-injection and organs were removed, weighed, and counted in a gamma counter for ⁸⁹Zr activity. The percent injected dose per gram (%ID g⁻¹) for each organ was computed by normalization to the total activity injected (decay-corrected).

Supporting Information

Supporting Information is available from the Wiley Online Library or from the author.

Acknowledgements

S.E.M. and J.L. thank the MAT2017-88752-R and CTQ2017-87637-R Retos projects, respectively, from the Ministerio de Economía, Industria y Competitividad, gobierno de España; G.S.-I. acknowledges support from ANPcyT (PICT 2015–2526 and PICT 2018–4651). This work was performed under the Maria de Maeztu Units of Excellence Program from the Spanish State Research Agency—Grant no. MDM-2017-0720.

Conflict of Interest

The authors declare no conflict of interest.

Author Contributions

E.B. and M.A.R. contributed equally to this work. E.B., M.A.R., S.M., J.L., and G.S.-I. conceived and designed the study. E.B. and M.A.R. synthesized and characterized mesoporous nanoparticles, performed the radioactive labeling, and the ex-vivo experiments. X.R. supervised the radio-labeling experiments and the ex-vivo experiments and performed the animal sacrifices. U.C. performed PET/CT scans. C.S. analyzed PET/CT data. V.G.-V. organized and supervised animal experiments. E.B., M.A.R., S.M., and J.L. analyzed and discussed the data. E.B., S.M., and J.L. contributed to the writing of this paper. All authors have read and approved the final manuscript.

Data Availability Statement

The data that support the findings of this study are available from the corresponding author upon reasonable request.

Keywords

biodistribution, degradation, in vivo imaging, mesoporous silica nanoparticles, radiolabeling

Received: March 15, 2021

Revised: April 2, 2021

Published online:

- [1] H. Shao, T.-J. Yoon, M. Liang, R. Weissleder, H. Lee, *Beilstein J. Nanotechnol.* **2010**, *1*, 142.
- [2] S. Prijic, G. Sersa, *Radiol. Oncol.* **2011**, *45*, 1.
- [3] L. Cong, M. Takeda, Y. Hamanaka, K. Gonda, M. Watanabe, M. Kumasaka, Y. Kobayashi, M. Kobayashi, N. Ohuchi, *PLoS One* **2010**, *5*, e13167.
- [4] J. E. Fuller, G. T. Zugates, L. S. Ferreira, H. S. Ow, N. N. Nguyen, U. B. Wiesner, R. S. Langer, *Biomaterials* **2008**, *29*, 1526.
- [5] M. N. Rhyner, A. M. Smith, X. Gao, H. Mao, L. Yang, S. Nie, *Nanomedicine* **2006**, *1*, 209.
- [6] X. Gao, Y. Cui, R. M. Levenson, L. W. K. Chung, S. Nie, *Nat. Biotechnol.* **2004**, *22*, 969.
- [7] E. Boisselier, D. Astruc, *Chem. Soc. Rev.* **2009**, *38*, 1759.
- [8] L. R. Hirsch, R. J. Stafford, J. A. Bankson, S. R. Sershen, B. Rivera, R. E. Price, J. D. Hazle, N. J. Halas, J. L. West, *Proc. Natl. Acad. Sci. U. S. A.* **2003**, *100*, 13549.
- [9] C. J. Gannon, C. Patra, R. Bhattacharya, P. Mukherjee, S. A. Curley, *J. Nanobiotechnol.* **2008**, *6*, 2.
- [10] R. Liang, M. Wei, D. G. Evans, X. Duan, *Chem. Commun.* **2014**, *50*, 14071.
- [11] M. Alhariri, A. Azghani, A. Omri, *Expert Opin. Drug Delivery* **2013**, *10*, 1515.
- [12] P. P. Deshpande, S. Biswas, V. P. Torchilin, *Nanomedicine* **2013**, *8*, 1509.
- [13] N. Doshi, S. Mitrugotri, *Adv. Funct. Mater.* **2009**, *19*, 3843.
- [14] W. B. Liechty, D. R. Kryscio, B. V. Slaughter, N. A. Peppas, *Annu. Rev. Chem. Biomol. Eng.* **2010**, *1*, 149.
- [15] H. Zhang, Z. Ji, T. Xia, H. Meng, C. Low-Kam, R. Liu, S. Pokhrel, S. Lin, X. Wang, Y.-P. Liao, M. Wang, L. Li, R. Rallo, R. Damoiseaux, D. Telesca, L. Mädler, Y. Cohen, J. I. Zink, A. E. Nel, *ACS Nano* **2012**, *6*, 4349.
- [16] C. Argyo, V. Weiss, C. Bräuchle, A. Bein, E. Thomas, *Chem. Mater.* **2014**, *26*, 435.
- [17] Y.-S. Lin, K. R. Hurley, C. L. Haynes, *J. Phys. Chem. Lett.* **2012**, *3*, 364.
- [18] F. Tang, L. Li, D. Chen, *Adv. Mater.* **2012**, *24*, 1504.
- [19] R. Narayan, U. Nayak, A. Raichur, S. Garg, *Pharmaceutics* **2018**, *10*, 118.
- [20] Y. Chen, H. Chen, J. Shi, *Adv. Mater.* **2013**, *25*, 3144.
- [21] Y. Zhao, B. G. Trewyn, I. I. Slowing, V. S.-Y. Lin, *J. Am. Chem. Soc.* **2009**, *131*, 8398.
- [22] H.-J. Kim, H. Matsuda, H. Zhou, I. Honma, *Adv. Mater.* **2006**, *18*, 3083.
- [23] C. Murugan, K. Rayappan, R. Thangam, R. Bhanumathi, K. Shanthi, R. Vivek, R. Thirumurugan, A. Bhattacharyya, S. Sivasubramanian, P. Gunasekaran, S. Kannan, *Sci. Rep.* **2016**, *6*, 34053.
- [24] Q. Fu, D. Hargrove, X. Lu, *Nanomed.: Nanotechnol., Biol. Med.* **2016**, *12*, 1951.
- [25] M. Ganesh, U. Ubaidulla, P. Hemalatha, M. M. Peng, H. T. Jang, *AAPS PharmSciTech* **2015**, *16*, 944.
- [26] K. Möller, K. Müller, H. Engelke, C. Bräuchle, E. Wagner, T. Bein, *Nanoscale* **2016**, *8*, 4007.
- [27] C. Tao, Y. Zhu, Y. Xu, M. Zhu, H. Morita, N. Hanagata, *Dalton Trans.* **2014**, *43*, 5142.
- [28] G. V. Deodhar, M. L. Adams, B. G. Trewyn, *Biotechnol. J.* **2017**, *12*, 1600408.
- [29] Silicon Dioxide GRAS Notification.
- [30] D. Bobo, K. J. Robinson, J. Islam, K. J. Thurecht, S. R. Corrie, *Pharm. Res.* **2016**, *33*, 2373.
- [31] E. Phillips, O. Penate-Medina, P. B. Zanzonico, R. D. Carvajal, P. Mohan, Y. Ye, J. Humm, M. Gonen, H. Kalaigian, H. Schoder, H. W. Strauss, S. M. Larson, U. Wiesner, M. S. Bradbury, *Sci. Transl. Med.* **2014**, *6*, 260ra149.
- [32] H. Yamada, C. Urata, Y. Aoyama, S. Osada, Y. Yamauchi, K. Kuroda, *Chem. Mater.* **2012**, *24*, 1462.
- [33] G. Chen, Z. Teng, X. Su, Y. Liu, G. Lu, *J. Biomed. Nanotechnol.* **2015**, *11*, 722.
- [34] L. Li, T. Liu, C. Fu, L. Tan, X. Meng, H. Liu, *Nanomed.: Nanotechnol., Biol. Med.* **2015**, *11*, 1915.
- [35] M. Manzano, V. Aina, C. O. Areán, F. Balas, V. Cauda, M. Colilla, M. R. Delgado, M. Vallet-Regí, *Chem. Eng. J.* **2008**, *137*, 30.
- [36] V. Cauda, C. Argyo, T. Bein, *J. Mater. Chem.* **2010**, *20*, 8693.
- [37] V. Cauda, A. Schlossbauer, T. Bein, *Microporous Mesoporous Mater.* **2010**, *132*, 60.
- [38] Y.-S. Lin, N. Abadeer, K. R. Hurley, C. L. Haynes, *J. Am. Chem. Soc.* **2011**, *133*, 20444.
- [39] S. P. Hadipour Moghaddam, R. Mohammadpour, H. Ghandehari, *J. Controlled Release* **2019**, *311*, 1.
- [40] M. Vallet-Regí, F. Balas, D. Arcos, *Angew. Chem., Int. Ed.* **2007**, *46*, 7548.
- [41] J. G. Croissant, Y. Fatiev, N. M. Khashab, *Adv. Mater.* **2017**, *29*, 1604634.
- [42] T. Fontecave, C. Sanchez, T. Azaïs, C. Boissière, *Chem. Mater.* **2012**, *24*, 4326.
- [43] R. Mortera, S. Fiorilli, E. Garrone, E. Verné, B. Onida, *Chem. Eng. J.* **2010**, *156*, 184.
- [44] P. M. Dove, N. Han, A. F. Wallace, J. J. De Yoreo, *Proc. Natl. Acad. Sci. U. S. A.* **2008**, *105*, 9903.
- [45] Q. He, J. Shi, M. Zhu, Y. Chen, F. Chen, *Microporous Mesoporous Mater.* **2010**, *131*, 314.
- [46] E. Bindini, Z. Chehadi, M. Faustini, P.-A. Albouy, D. Grosso, A. Cattoni, C. Chanéac, O. Azzaroni, C. Sanchez, C. Boissière, *ACS Appl. Mater. Interfaces* **2020**, *12*, 13598.
- [47] R. O. Fournier, J. J. Rowe, *Am. Mineral.* **1977**, *62*, 1052.
- [48] G. B. Alexander, W. M. Heston, R. K. Iler, *J. Phys. Chem.* **1954**, *58*, 453.
- [49] S.-A. Yang, S. Choi, S. M. Jeon, J. Yu, *Sci. Rep.* **2018**, *8*, 185.

- [50] K. Braun, A. Pochert, M. Beck, R. Fiedler, J. Gruber, M. Lindén, *J. Sol-Gel Sci. Technol.* **2016**, *79*, 319.
- [51] Y.-S. Lin, N. Abadeer, C. L. Haynes, *Chem. Commun.* **2011**, *47*, 532.
- [52] S. Goel, F. Chen, S. Luan, H. F. Valdovinos, S. Shi, S. A. Graves, F. Ai, T. E. Barnhart, C. P. Theuer, W. Cai, *Adv. Sci.* **2016**, *3*, 1600122.
- [53] J. D. Bass, D. Grosso, C. Boissiere, E. Belamie, T. Coradin, C. Sanchez, *Chem. Mater.* **2007**, *19*, 4349.
- [54] T. Asefa, Z. Tao, *Chem. Res. Toxicol.* **2012**, *25*, 2265.
- [55] J. M. Rosenholm, V. Mamaeva, C. Sahlgren, M. Lindén, *Nanomedicine* **2012**, *7*, 111.
- [56] P. Dogra, N. L. Adolphi, Z. Wang, Y.-S. Lin, K. S. Butler, P. N. Durfee, J. G. Croissant, A. Noureddine, E. N. Coker, E. L. Bearer, V. Cristini, C. J. Brinker, *Nat. Commun.* **2018**, *9*, 4551.
- [57] F. Chen, S. Goel, H. F. Valdovinos, H. Luo, R. Hernandez, T. E. Barnhart, W. Cai, *ACS Nano* **2015**, *9*, 7950.
- [58] F. Chen, K. Ma, L. Zhang, B. Madajewski, P. Zanzonico, S. Sequeira, M. Gonen, U. Wiesner, M. S. Bradbury, *Chem. Mater.* **2017**, *29*, 8269.
- [59] F. Garbassi, L. Balducci, R. Ungarelli, *J. Non-Cryst. Solids* **1998**, *223*, 190.
- [60] J. M. Kim, S. M. Chang, S. Kim, K.-S. Kim, J. Kim, W.-S. Kim, *Ceram. Int.* **2009**, *35*, 1243.
- [61] T. M. Shaffer, M. A. Wall, S. Harmsen, V. A. Longo, C. M. Drain, M. F. Kircher, J. Grimm, *Nano Lett.* **2015**, *15*, 864.
- [62] Q. He, Z. Zhang, F. Gao, Y. Li, J. Shi, *Small* **2011**, *7*, 271.
- [63] D. S. Abou, T. Ku, P. M. Smith-Jones, *Nucl. Med. Biol.* **2011**, *38*, 675.
- [64] J. Lu, M. Liong, Z. Li, J. I. Zink, F. Tamanoi, *Small* **2010**, *6*, 1794.
- [65] C.-H. Lee, S.-H. Cheng, Y.-J. Wang, Y.-C. Chen, N.-T. Chen, J. Souris, C.-T. Chen, C.-Y. Mou, C.-S. Yang, L.-W. Lo, *Adv. Funct. Mater.* **2009**, *19*, 215.
- [66] J. S. Souris, C.-H. Lee, S.-H. Cheng, C.-T. Chen, C.-S. Yang, J. A. Ho, C.-Y. Mou, L.-W. Lo, *Biomaterials* **2010**, *31*, 5564.
- [67] H. Meng, M. Xue, T. Xia, Z. Ji, D. Y. Tarn, J. I. Zink, A. E. Nel, *ACS Nano* **2011**, *5*, 4131.